Measurement of Electron Density and Temperature Using Laser Thomson Scattering in PANTA

Kentaro TOMITA[1)], Yuta SATO[1)], Nima BOLOUKI[1)], Tatsuro SHIRAISHI[1)], Kiichiro UCHINO[1)], Yudai MIWA[1,2)], Tatsuya KOBAYASHI[3)] and Shigeru INAGAKI[1,2)]

[1)]*Interdisciplinary Graduate School of Engineering Sciences, Kyushu University, Fukuoka 816-8580, Japan*
[2)]*Research Institute for Applied Mechanics, Kyushu University, Fukuoka 816-8580, Japan*
[3)]*National Institute for Fusion Science, Gifu 509-5292, Japan*

(Received 4 November 2016 / Accepted 17 March 2017)

Electron density (n_e) and electron temperature (T_e) measurements were performed via the plasma assembly for nonlinear turbulence analysis (PANTA) using the laser Thomson scattering technique. The second harmonic of Nd:YAG laser (λ = 532 nm) and an intensified charge-coupled device were used as a light source and a detector, respectively. Plasmas in PANTA were generated with Ar gas in a pressure range of 1 - 5 mTorr. The range of the applied magnetic field was 600 - 1500 G. At the center of the plasma, n_e and T_e ranged (4 - 20) $\times$ 10^{18} m^{-3} and 0.8 - 3 eV, respectively. Further, n_e monotonically increased and T_e monotonically decreased with the increasing gas pressure and magnetic field.

Keywords: PANTA, laser Thomson scattering, electron density, electron temperature, Ar plasma

DOI: 10.1585/pfr.12.1401018

1. Introduction

Basic plasma experiments are very useful for investigating the fundamental physical processes in magnetized plasma. The high accessibility of such basic experimental devices allows us to realize simultaneous multi-point measurement using Langmuir probes. The spatial and temporal resolutions of such measurements meet the requirements for studies on nonlinear plasma dynamics. However, there are concerns regarding the effects of insertion of the probes on plasma. In addition, many factors (e.g., presence of a magnetic field [1] and secondary electron emission from the probe surface [2]) can break a simple probe theory. Therefore, to verify probe measurement in basic plasmas, another diagnostic is required.

Laser Thomson scattering (LTS) is widely known as a reliable technique for the nonintrusive simultaneous measurement of electron density (n_e) and electron temperature (T_e) for various types of plasmas, such as magnetic confinement fusion plasmas [3], low-temperature plasmas for industrial applications [4–6], laser-produced plasmas [7–9], and others [10].

For a more precise understanding of magnetized plasma phenomena, accurate radial profiles of n_e and T_e are essential. For example, the observed equilibrium n_e and T_e are used for simulating turbulence in the basic plasma [9]; then, the calculated turbulence spectra are compared with the experimental observations. The turbulence spectrum in the linear magnetized plasma changes depending on the operational conditions (neutral gas pressure and magnetic field) in the plasma assembly for nonlinear turbulence analysis (PANTA) and LMD-U [11]. A linear plasma simulator was developed, and qualitative comparisons between the simulation results and experimental observations have commenced [12]. For more comprehensive understanding of plasma turbulence, a quantitative comparison is required. Moreover, turbulent spectra are strongly influenced by the local mean parameters and their gradients. Accordingly, in this work, we observed n_e and T_e in the central region, which cannot be accessed by a probe, under the wide operational conditions using the LTS technique.

2. Experimental Setup

The experiment was conducted in PANTA, which is a linear magnetic field device [13]. In PANTA, cylindrical argon plasmas (diameter 0.1 m and length 4 m) are produced with a helicon wave (13.56 MHz, 3 kW) using a double-loop antenna around a quartz tube. Previous results obtained from several probe methods indicate that n_e and T_e in PANTA range approximately 0.5 - 1 $\times$ 10^{19} m^{-3} and 1 - 3 eV, respectively. For such ranges of n_e and T_e, the predicted Thomson scattering spectra from PANTA plasma are in the non-collective regime when a visible-wavelength laser is used as a probing laser [14]. The predicted LTS signal per one laser shot is small. However, accurate LTS measurements are possible with signal accumulation methods as done in many previous studies [4, 5, 15, 16]. Figure 1 shows the schematic of the PANTA and LTS systems. The second harmonics beam (λ = 532 nm) of

author's e-mail: tomita@ence.kyushu-u.ac.jp

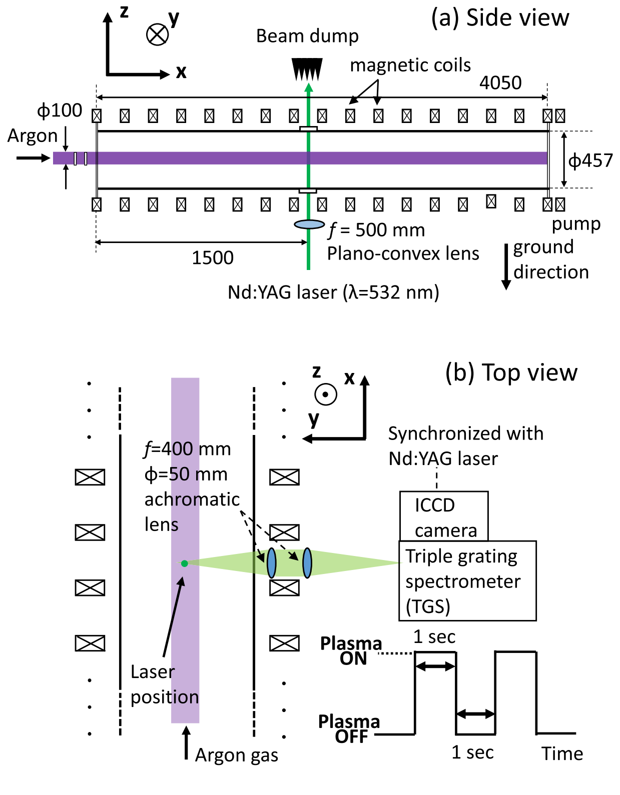

Fig. 1 Schematic of the PANTA and LTS systems. (a) Side view and (b) top view.

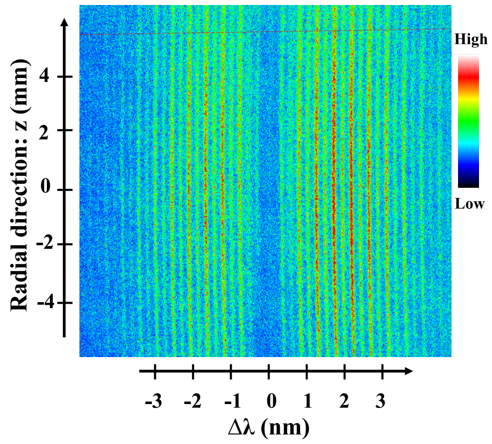

Fig. 2 Image of the rotational Raman scattering spectra of nitrogen molecule under 100 Torr gas pressure.

the Nd:YAG laser (Continuum, Surelite III, laser energy 130 mJ at $\lambda = 532$ nm) was used as the light source. The pulse duration and repetition rate of the probing laser were 10 ns and 10 Hz, respectively. The probing laser was injected into the PANTA plasma via a quartz window installed at the bottom of the vacuum vessel of PANTA. The laser beam was focused at the center of the vessel by means of a plano-convex lens ($f = 500$ mm, $\phi = 25.4$ mm). The spot size of the laser beam was 200 µm full width at half maximum, which was estimated from the measurements of Rayleigh scattering of nitrogen gas. Light scattered from the laser path with a scattering angle of 90° was focused onto the entrance slit (width 0.2 mm) of the triple grating spectrometer (TGS) with two achromatic lenses (effective diameter 45 mm) with focal lengths of $f = 400$ mm, as shown in Fig. 1 (b). Because the basic configuration of the TGS has been already reported in many studies [4, 5, 17], only a brief explanation is presented here.

The TGS mainly comprises six achromatic lenses ($f = 250$ mm, diameter 46 mm), three diffraction gratings (2400 lines/mm), an entrance slit (width 0.2 mm), a physical notch filter (width 0.5 mm) at the first image plane, and an intermediate slit (width 0.2 mm) at the second image plane. In the TGS, light is dispersed by the first grating and focused on the physical notch filter, which blocks light with $\lambda = 532$ nm. The light that passes through the notch filter is then sent to the second grating, which recombines the dispersed spectrum into a single beam. Then, the light is refocused on the intermediate slit. The light that passes through the intermediate slit is dispersed again by the third grating and detected by an intensified charge-coupled device (ICCD) camera (Princeton Instruments, PI-MAX, quantum efficiency: 35% at $\lambda = 532$ nm). The instrumental function of the TGS was 0.2 nm. The transmission coefficient of the TGS was evaluated to be approximately 30%.

The probing laser was injected into the plasma at 10 Hz. Because of the small intensity of LTS, 3000 shot accumulation was performed for one measurement event. In this study, the duty ratio of plasma operation was 1 : 1, as shown in Fig. 1 (b). This means that only half of the laser shots can hit the plasma. Therefore, the substantial accumulated number of the laser shot was 1500 for one measurement. The plasma was produced at three gas pressures of Ar, 1, 3, and 5 mTorr. In addition, observations were made for three values of induction of the applied magnetic field (600, 900, and 1500 G). In other words, plasma was produced under nine conditions.

Before producing the plasmas and measuring the Thomson scattering spectra, the rotational Raman scattering spectra for nitrogen gas at 100 Torr were measured. The Raman scattering measurement was performed to calibrate the LTS system from the viewpoints of wavelength dispersion and relative signal intensity along the z axis [18–21]. Figure 2 shows the result of Raman scattering. In the figure, $\Delta\lambda$ is difference in wavelength from the probing laser wavelength. As shown in this figure, because the direction of the entrance slit of the TGS (height 10 mm) corresponds to the direction of the incident laser path, one-dimensional [z axis as shown in Fig. 1 (a)] spatially resolved measurements were achieved simultaneously. Figure 3 shows the Thomson scattering spectrum of the plasma produced under a magnetic field of 1500 G and Ar gas pressure of 5 mTorr. The dark area observed around the wavelength of the probing laser is attributed to the physical notch filter inside the TGS, which blocked light near the laser wavelength (±0.4 nm from the laser wavelength). Using this TGS, the clear Thomson scattering spectra 0.4 nm away from the probe laser were obtained without the problem of stray light. The LTS signals were plotted against $(\Delta\lambda)^2$ using a logarithmic scale for the ordinate, where $(\Delta\lambda)^2$ is proportional to the electron energy. Figure 4 shows the spatially integrated LTS spectra in the range $-2 < z < 2$ mm corresponding to Fig. 3. This figure shows that the Thomson scattering spectra were linear for energies ranging from 1 to 4 eV, which correspond to the value of $(\Delta\lambda)^2$ from 2.2 nm^2 to 8.8 nm^2. This slope means that the electron energy distribution function (EEDF) was Maxwellian in this range of energies. T_e was determined by Gaussian fittings of the LTS spectra in this energy region. To obtain n_e, an absolute calibration of the LTS signal was performed by measuring the Rayleigh scattering [22] from the vacuum chamber when it was filled with nitrogen gas at around atmospheric pressure.

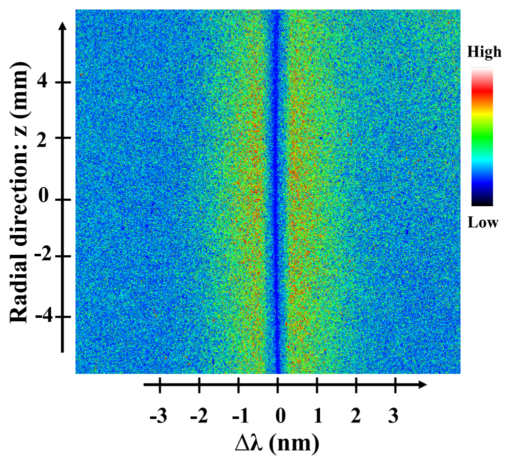

Fig. 3 The LTS spectra of PANTA plasma produced in a magnetic field of 1500 G and 5 mTorr Ar gas.

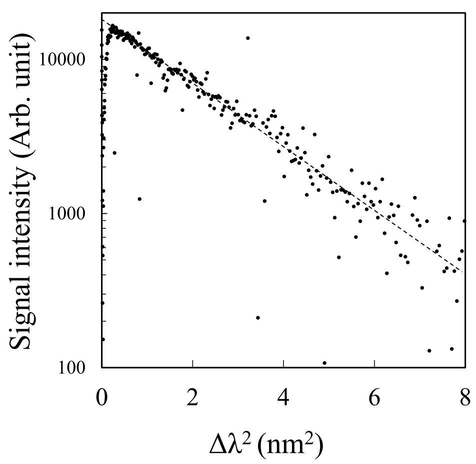

Fig. 4 Thomson scattering spectra extracted from $-2 < z < 2$ mm in Fig. 3.

3. Results and Discussion

The operation ranges of B and p_{Ar} in this experiment were 600 - 900 G and 1 - 5 mTorr, respectively. The T_e and n_e measured by LTS are compared with those measured by the double-probe method. Figure 5 shows the typical radial profiles of T_e and n_e in the standard PANTA plasma (B = 900 G and p_{Ar} = 1 mTorr). Probe measurements were performed in the plasma under identical operational conditions. The error-bars in the graphs of T_e and n_e measured with the probe denote the standard deviations of the curve-fitting parameters. Although the probe cannot access to the central region of the plasma considering the large insertion effect on plasma (significant decrease in density), the LTS results are in good agreement with the values extrapolated from the probe results. In the ionization equilibrium state of Ar plasma, Ar^+ is the major ion species (ionic fraction of Ar^{2+} is more than 100 times lower than that of Ar^+) when T_e is less than 2.5 eV [23]. Thus, the contribution of Ar^{2+} to electron density is considered negligible. A previous study also demonstrated the good agreement between the probe method and LTS diagnostics for electron density measurement [10].

Figure 6 shows the central n_e and T_e of the plasmas produced under different operational conditions. As shown in Fig. 6 (b), T_e decreased with an increase in P_{Ar}, and the B dependence of T_e was weak. The central n_e monotonically increased with an increase in B and P_{Ar}. The increase in n_e is qualitatively explained by the increase in the ionization frequency through the increase in the gas density. On the other hand, the central ionization ratio monotonically

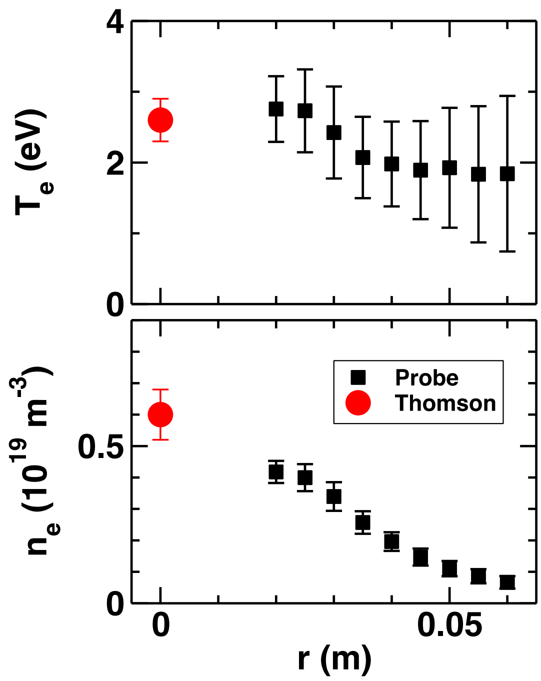

Fig. 5 Radial profiles of T_e and n_e. The double-probe, which can move in the radial direction, was installed at z = 1.625 m.

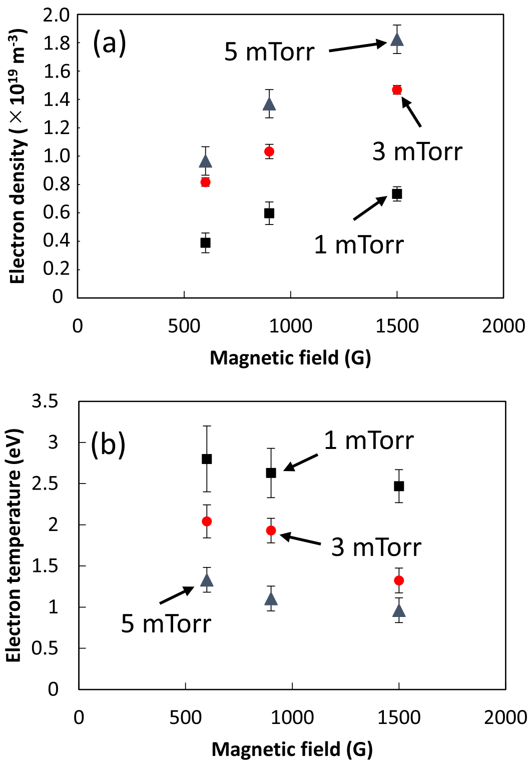

Fig. 6 (a) Electron density and (b) electron temperature of PANTA plasmas produced with different magnetic fields and Ar gas pressures.

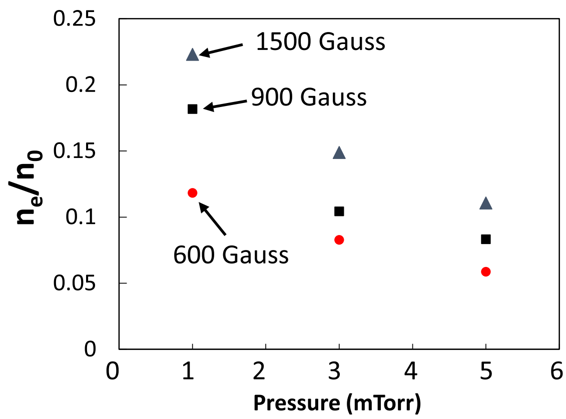

Fig. 7 Degree of ionization calculated from the LTS results shown in Fig. 6 (b).

decreased with increase in P_{Ar}. Figure 7 shows the degree of ionization (n_e/n_0), where n_0 is the neutral atom density and is estimated by the neutral argon pressure based on the assumption of uniform spatial distribution of Ar atoms at room temperature. The degree of ionization increased with an increase in B. This is attributed to the improvement of electron confinement in higher B. Figure 8 shows the B dependence of central electron pressure (n_eT_e). The central pressure increases with an increase in B and tends to saturate in the strong magnetic field region (~1500 G). The P_{Ar}

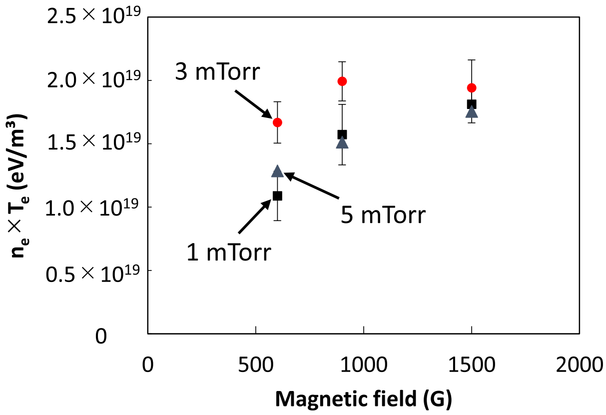

Fig. 8 Central electron pressure as calculated from the LTS results shown in Figs. 6 (a) and 6 (b).

dependence of the central pressure is not monotonic. The central electron pressure generated at P_{Ar} = 3 mTorr was the highest at all operating magnetic fields in our investigations. These observations suggest that the radial profile of electron pressure changed significantly depending on the operational conditions of PANTA plasma. The radial structure can be observed in a future work.

The n_e and T_e obtained in this study are time-integrated values. However, turbulence was generated in the PANTA plasmas. Measurement of turbulent n_e and T_e fluctuations is important to identify the instability in plasma and evaluate the particle and heat transport driven by the turbulence. For time-resolved measurement, the conditional averaging technique can be used [24]; that is, in PANTA, a strong quasi-coherent mode is excited in the low-frequency region. These low-frequency components of T_e and n_e are extracted by the conditional averaging technique. In this technique, the fluctuation signal monitored with a probe is bandpassed, and the periods at which the waveform of the fundamental frequency crosses the zero level are picked up to trigger the laser. This process is performed by a signal processing system with a field-programmable gate array. The probing laser is shot synchronized with the trigger, and a few hundred shots of Thomson scattering are averaged to evaluate n_e and T_e. By changing the delay between the trigger and probing laser, the averaged temporal evolution of T_e and n_e synchronized with the low-frequency fluctuation can be obtained.

In a future LTS system, to achieve an accurate LTS measurement with the accumulation of only a few hundred laser shots, both the laser energy and solid angle of the collecting lenses will be doubled. In addition, a new ICCD camera (PI-MAX4) with high quantum efficiency (>45% at λ = 532 nm) will be used.

4. Conclusion

LTS was applied to the PANTA plasma for the measurement of time-integrated n_e and T_e at the center of the plasma. Results clearly show that n_e increased with increasing magnetic field and Ar gas pressure. On the other hand, T_e slightly decreased with increase in the Ar gas pressure. Precise measurement of the absolute values of n_e and T_e under different experimental conditions demonstrated that this LTS system is useful for PANTA plasma diagnostics.

We are grateful to Mr. Mutaguchi for his technical support. This work is partially supported by the collaboration programs of RIAM of Kyushu University.

[1] S. Teii, *Plasma Kisokougaku* [*Plasma Engineering Science*], Sec. 3 (Uchida Rokakuho 1995).
[2] S.-L. Chen, J.-S. Chang and S. Matsumura, J. Appl. Phys. **41**, 1711 (1970).
[3] W.C. Young and D. Parfeniuk, Rev. Sci. Instrum. **87**, 11E521 (2016).
[4] K. Muraoka and A. Kono, J. Phys. D. Appl. Phys. **44**, 43001 (2011).
[5] A. Kono and K. Iwamoto, Jpn. J. Appl. Phys. **43**, L1010 (2004).
[6] M.J. van de Sande, *Laser Scattering on Low Temperature Plasmas—High Resolution and Stray Light Rejection*, Eindhoven, Eindhoven University of Technology, Ph. D thesis (2002).
[7] K. Tomita, K. Nakayama, K. Inoue, A. Sunahara and K. Uchino, Appl. Phys. Express **6**, 076101 (2013).
[8] D. Froula, L. Divol and S. Glenzer, Phys. Rev. Lett. **88**, 105003 (2002).
[9] T. Morita, Y. Sakawa, K. Tomita, T. Ide, Y. Kuramitsu, K. Nishio, K. Nakayama, K. Inoue, T. Moritaka, H. Ide, M. Kuwada, K. Tsubouchi, K. Uchino and H. Takabe, Phys. Plasmas **20**, 92115 (2013).
[10] A. Okamoto *et al.*, Contrib. Plasma Phys. **46**, No.5-6, 416 (2006).
[11] H. Arakawa *et al.*, Plasma Phys. Control. Fusion **52**, 105009 (2010).
[12] M. Sasaki, N. Kasuya, K. Itoh, M. Yagi and S.-I. Itoh, Nucl. Fusion **54**, 114009 (2014).
[13] S. Inagaki, T. Kobayashi, Y. Kosuga, S.-I. Itoh, T. Mitsuzono, Y. Nagashima, H. Arakawa, T. Yamada, Y. Miwa, N. Kasuya, M. Sasaki, M. Lesur, A. Fujisawa and K. Itoh, Sci. Rep. **6**, 22189 (2016).
[14] J. Sheffield, D. Froula, S.H. Glenzer and N.C. Luhmann Jr., *Plasma Scattering of Electromagnetic Radiation, 2nd Edition* (Academic Press, 2010).
[15] S. Hübner, S. Hofmann, E.M. van Veldhuizen and P.J. Bruggeman, Plasma Sources Sci. Technol. **22**, 65011 (2013).
[16] W. Chen, K. Ogiwara, K. Koge, K. Tomita, K. Uchino and Y. Kawai, Plasma Fusion Res. **8**, 1306114 (2013).
[17] S. Hassaballa, M. Yakushiji, Y.K. Kim, K. Tomita, K. Uchino and K. Muraoka, IEEE Trans. Plasma Sci. **32**, 127 (2004).
[18] K. Tomita, K. Urabe, N. Shirai, Y. Sato, S. Hassaballa, N. Bolouki, M. Yoneda, T. Shimizu and K. Uchino, Jpn. J. Appl. Phys. **55**, 66101 (2016).
[19] A.F.H. van Gessel, E.A.D. Carbone, P.J. Bruggeman and J.J.A.M. van der Mullen, Plasma Sources Sci. Technol. **21**, 15003 (2012).
[20] I. Yamada, K. Narihara, H. Hayashi, H. Funaba and LHD experimental group, Plasma Fusion Res. **2**, S1106 (2007).
[21] R. Scannell, M. Beurskens, M. Kempenaars, G. Naylor, M. Walsh, T. O'Gorman and R. Pasqualotto, Rev. Sci. Instrum. **81**, 1 (2010).
[22] R. Thalman, K.J. Zarzana, M.A. Tolbert and R. Volkamer, J. Quant. Spectrosc. Radiat. Transf. **147**, 171 (2014).
[23] M. Arnaud and R. Rohtenflug, Astron. Astrophys. Suppl. Ser. **60**, 425 (1985).
[24] S. Inagaki, Y. Miwa, T. Kobayashi, T. Yamada, Y. Nagashima, T. Mitsuzono, H. Fujino, M. Sasaki, N. Kasuya, M. Lesur, Y. Kosuga, A. Fujisawa, S.-I. Itoh and K. Itoh, Plasma Fusion Res. **9**, 3 (2014).